

RSC Advances



This is an *Accepted Manuscript*, which has been through the Royal Society of Chemistry peer review process and has been accepted for publication.

Accepted Manuscripts are published online shortly after acceptance, before technical editing, formatting and proof reading. Using this free service, authors can make their results available to the community, in citable form, before we publish the edited article. This *Accepted Manuscript* will be replaced by the edited, formatted and paginated article as soon as this is available.

You can find more information about *Accepted Manuscripts* in the [Information for Authors](#).

Please note that technical editing may introduce minor changes to the text and/or graphics, which may alter content. The journal's standard [Terms & Conditions](#) and the [Ethical guidelines](#) still apply. In no event shall the Royal Society of Chemistry be held responsible for any errors or omissions in this *Accepted Manuscript* or any consequences arising from the use of any information it contains.

Interface instabilities and chaotic rheological responses in binary polymer mixtures under shear flow

Xiaowei Guo,^{ab} Shun Zou,^a Xuejun Yang,^a Xue-Feng Yuan^{*ba} and Miao Wang^a

Received Xth XXXXXXXXXXXX 20XX, Accepted Xth XXXXXXXXXXXX 20XX

First published on the web Xth XXXXXXXXXXXX 200X

DOI: 10.1039/b000000x

A unified model by combining the Rolie-Poly constitutive model and the Flory-Huggins mixing free energy functional through a two fluid approach is presented for studying flow-induced phase separation in polymer mixtures. It is numerically solved in two-dimensional flow with monotonic and non-monotonic constitutive behaviour. The results are analyzed and show that this model can capture the essential dynamic features of viscoelastic phase separation reported in literature. The steady-state shear-banding and interface instabilities are reproduced. In the case with a non-monotonic constitutive behaviour, it is observed that the band structures are strongly unstable both in time and in space. The correlations between the microstructure evolution and chaotic rheological responses have been identified. A vortex structure emerges within the central band. Numerical results obtained from this study suggest that the dynamic features of rheochaos can be captured by the proposed model without introducing extra parameters.

1 Introduction

Shear-induced phase separation in complex fluids has attracted great attention over the last decade. Nearly 60 years ago, it was observed¹ that phase transitions of polymer solutions are influenced by flow. Since then there have been many reports on shear-induced phase separation of polymer mixtures and other complex fluids^{2–7}. As a closely related phenomenon, shear-banding was also observed in numerous publications, recent experiments include wormlike micelles^{8,9}, telechelic polymers^{10,11}, dispersions¹² and entangled DNA solutions^{13–15}.

A typical experimental system targeted by this work is the Couette cell described in Ref⁸. Fluids are contained in the gap between the stationary inner cylinder and the rotating outer cylinder. Various shear rates are applied by superimposing different angular velocities to the rotating cylinder. Focused on the bulk fluid behaviour, we simulate the shear flow in a rectangular region. A commonly accepted idea is that the flow field can cause stress imbalance between different components of polymer mixtures and relative motion can thus take place. By an adequate formulation of polymer blends, and careful control of temperature and flow fields, it is possible to manipulate the morphology of materials in micromorphological engineering.

Phase separations in classical binary fluids have been extensively studied both experimentally and theoretically over several decades¹⁶. Theoretical frameworks for modelling the effect of flow on phase transitions in polymer mixtures must incorporate both thermodynamic and viscoelastic forces into dynamic equations. Most theoretical research are based on the two fluid model, which combines thermodynamics, hydrodynamics, and viscoelasticity in a natural, physical way.

Few numerical results were presented for the two fluid model, especially regarding the effects of flow on phase diagram. Most of the early solutions of the two fluid model were obtained from approximations to the model, such as linearization of the diffusive equation and the adiabatic approximation^{17–19}, in which time dependence of the viscoelastic stress tensor was not considered to seek a possible steady state solution. Some recent research^{20–22} aim to numerically study the phase separation in a binary fluid, and large scale 2D and 3D simulations are carried out, but in absence of a realistic constitutive model, all of them can not accurately capture the viscoelastic effects. Modeling the phase separation in viscoelastic complex fluids with a realistic model remains elusive.

Jupp and Yuan^{23–25} presented a two fluid model (FH-JS model) to investigate the flow-induced phase mixing and demixing of polymer mixtures, which coupled the Flory-Huggins mixing free energy function and the Johnson-Segalman constitutive model in a unified way. The numerical results were obtained by solving the time-dependent two fluid model without any simplification used widely in early studies. Fielding and Olmsted^{26,27} proposed a different version of the two fluid model for the coupling between shear banding

^a State Key Laboratory of High Performance Computing, National University of Defense Technology, Changsha, Hunan, China

^b School of Chemical Engineering and Analytical Science, Manchester Institute of Biotechnology, University of Manchester, Manchester, M13 9PL, United Kingdom; E-mail: xuefeng.yuan@nscg-gz.cn

and shear-induced demixing, which still retained a diffusive stress term in the J-S constitutive equation. It is questionable whether or not such an ad-hoc treatment for mechanical interface is justifiable as the origin of the diffusive stress is molecular diffusion across the streamlines and has already been considered in a thermodynamically consistent way in the original two fluid model.

Moreover, the J-S model is a phenomenological constitutive model. The Rolie-Poly model²⁸ is a simplified version of the full molecular model based on the tube dynamics²⁹, yet still includes all dynamic modes considered in the full theory, including the reptation, chain stretch, contour length fluctuation, and thermal/convective constraint releases (CCR). Many numerical results^{30–33} were carried out using a diffusive Rolie-Poly model, which verified that the Rolie-Poly constitutive model has the capability to accurately capture the rheological responses in a complex fluid. Recently, Cromer³⁴ predicted the steady-state shear-banding with Rolie-Poly constitutive model for a monodisperse polymer solution, which coupled the concentration/stress through a two-fluid approach, but only one-dimensional calculations had been presented. To the best of our knowledge, this is the first attempt to couple the Rolie-Poly constitutive model with a two fluid model without adding a diffusive stress term. However, compared to Cromer's model, the framework of FH-JS model^{23–25} is more general and can model not only the polymer solutions with a reduced formulation but also the binary polymer mixtures in which both of components are viscoelastic.

In this study, the FH-JS model is modified by replacing the J-S constitutive model with the Rolie-Poly model. It is not only inherent all the advantages of the original model, but also can accurately capture polymer dynamics in flow-induced phase separation. Simulation work focuses on the shear-induced phase transition of polymer mixtures in which the volume fractions of the two components are equal. Both of transient and steady-state phase transition behaviour and corresponding rheological responses will be presented. In some cases, rather than reaching a steady state, the numerical results show erratic fluctuations. This phenomenon, often named as rheochaos, has been observed in many complex fluids, including wormlike micelles^{35–37}, associative polymer networks¹¹ and lamellar phase systems^{38,39}. In order to capture the key features of chaotic flows, several models^{40,41} have been studied by introducing some coupling parameters between flow and microstructure. Numerical results presented in this study demonstrate that the dynamic features of rheochaos can be captured by our model without introducing any extra parameters. The correlations between microstructure evolution and chaotic rheological responses are also identified.

The remainder of the paper is organized as follows. In the next section a detailed description of the two fluid model integrated with the Rolie-Poly constitutive model is presented.

Numerical Simulation results and discussions are provided in Section 4, in which the dynamic phase separation and rheological behaviour for both monotonic and non-monotonic constitutive relationships are analyzed through numerical simulations implemented using finite volume method. Section 5 contains our conclusions.

2 A two-fluid model integrated with Rolie-Poly constitutive model

Here we focused on the strong flow regime, as in such regime the viscoelastic and hydrodynamic forces completely dominate over the forces originated from the thermal fluctuations, it is therefore justifiable to neglect the effects of the thermal fluctuations as we did in the previous work^{23–25}.

To establish a theoretical framework for describing the phase separations of polymer blends, we coupled the Flory-Huggins free energy function with the Rolie-Poly constitutive model. The two-fluid model provides a physical approach to capture the inhomogeneous polymer dynamics. In the standard framework of the two-fluid model, the system consist of two components: the polymer and the solvent. A constitutive equation is required to describe the viscoelastic stress of the polymer component, and the solvent is pure Newtonian.

Compared to the original two-fluid approach^{19,42,43}, there are two main distinctions in our model. Firstly, both components are viscoelastic, and some mixing rules are introduced for calculation of the viscoelastic stress. This general formulation for binary polymer mixtures can be easily reduced to the standard two-fluid framework. Secondly, we replace the phenomenological constitutive model with a molecular-based model: Rolie-Poly model, which can provide more realistic predictions of the viscoelastic response under flow.

For polymer blends with two components, let $\phi_A(\vec{r}, t)$ and $\phi_B(\vec{r}, t)$ be the volume fractions of the component A and component B at some point \vec{r} and time t , and let $\vec{v}_A(\vec{r}, t)$ and $\vec{v}_B(\vec{r}, t)$ be their velocities, respectively. The volume average velocity \vec{v} is given by $\vec{v}(\vec{r}, t) = \phi_A \vec{v}_A(\vec{r}, t) + \phi_B \vec{v}_B(\vec{r}, t)$. The evolution equation for the volume fraction follows is given by the conservation law of mass, and may be written in terms of the volume average velocity:

$$\frac{\partial \phi_A(\vec{r}, t)}{\partial t} = -\vec{v} \cdot \vec{\nabla} \phi_A + \vec{\nabla} \cdot \left[\frac{\phi_A^2 \phi_B^2}{\zeta} (\vec{\nabla} \mu - \alpha \vec{\nabla} \cdot \boldsymbol{\sigma}_{ve}) \right] \quad (1)$$

The essential term of Eq. (1) can be expressed by the velocity difference between the two components, which depends on the osmotic force, $\vec{\nabla} \mu$ and the force due to inhomogeneity in polymer viscoelastic stress, $\vec{\nabla} \cdot \boldsymbol{\sigma}_{ve}$:

$$\vec{v}_A - \vec{v}_B = \frac{\phi_A \phi_B}{\zeta} \left[-\vec{\nabla} \mu + \alpha \vec{\nabla} \cdot \boldsymbol{\sigma}_{ve} \right] \quad (2)$$

where $\zeta = \zeta_A \zeta_B / (\zeta_A + \zeta_B)$ is a frictional coefficient. Following the Doi and Onuki's argument⁴² in their two fluid model for polymer mixtures, the friction coefficient may be expressed as $\zeta_i = \phi_i \zeta_{0i} M_i / M_{ei}$ ($i \in \{A, B\}$, ζ_{0i} and M_{ei} are the microscopic friction constant and the entanglement molecular weight for component i , respectively). For simplicity, we assume $\zeta_{0i} = \zeta_0$.

For the polymer inhomogeneity, we introduce a dimensionless coefficient α , and different from the previous work, the ratio of relaxation times is replaced by the ratio of the entanglements number,

$$\alpha = \frac{1 - G'Z'}{\phi_A + G'Z'\phi_B} \quad (3)$$

where the coefficient is related to the ratio of the modulus ($G' = G_B/G_A$) and the ratio of the entanglements number ($Z' = Z_B/Z_A$). $Z_i = M_i/M_e^i$ is the number of entanglements of each component polymer, and can be calculated by Rouse relaxation time τ_R^i and disentanglement relaxation time τ_d^i as $Z_i = \tau_d^i/(3\tau_R^i)$. This coefficient vanishes for $G'Z' = 1$, which includes the special case of a rheologically homogeneous system, where $G' = 1$ and $Z' = 1$. The viscoelastic force term, with the dimensionless coefficient α , can work either to oppose or to reinforce the thermodynamic force in the diffusive dynamics.

The osmotic force can be computed by the chemical potential difference μ , which is defined as the functional derivative of the mixing free energy with respect to local volume fraction, i.e.,

$$\mu = \frac{\delta \mathcal{F}_{\text{mix}}[\phi_A(\vec{r})]}{\delta \phi_A(\vec{r})} = - \frac{\delta \mathcal{F}_{\text{mix}}[\phi_B(\vec{r})]}{\delta \phi_B(\vec{r})}. \quad (4)$$

Here we take the first order approximation of Flory-Huggins free energy function form^{44,45} as

$$\mathcal{F}_{\text{mix}}[\phi_A(\vec{r})]/k_B T = \int d\vec{r} \left\{ f_{\text{mix}} k_B T + (\Gamma/2) [\nabla \phi_A]^2 \right\} \quad (5)$$

where Γ is the interfacial tension coefficient and any dependence of Γ on ϕ_A is ignored, and the equilibrium phase behavior can be defined by the Flory-Huggins mixing free energy, $f_{\text{mix}}/k_B T = (1/M_A) \phi_A \ln \phi_A + (1/M_B) \phi_B \ln \phi_B + \chi \phi_A \phi_B$, where M_i is the molecular weight of each component polymer and χ is the Flory-Huggins interaction parameter.

Apart from the osmotic force, another force the polymer experiences is the viscoelastic stress $\sigma_{\text{ve}}(\vec{r}, t)$, which can be calculated by constitutive equations. In our model, we replace the original JS model with the Rolie-Poly model. As the stress in entangled polymer systems is supported by chain molecules, a stress gradient would create a net force on the chains resulting in their relative migration. Thus $\vec{\nabla} \vec{v}_T$ should be used in the viscoelastic constitutive equation rather than $\vec{\nabla} \vec{v}$.

The tube velocity given by $\vec{v}_T = (\zeta_A \vec{v}_A + \zeta_B \vec{v}_B) / (\zeta_A + \zeta_B)$, may be expressed in terms of the volume average velocity by

$$\vec{v}_T = \vec{v} + \phi_A \phi_B \alpha (\vec{v}_A - \vec{v}_B) \quad (6)$$

where $(\vec{v}_A - \vec{v}_B)$ is defined by Eq. (2).

The relaxation modulus of a binary viscoelastic fluid must depend on its composition. For polymer linear blend, the relaxation modulus may be described as $G(t) = G_R(t) + G_d(t)$, where $G_R(t)$ describes the high-frequency polymer relaxation (Rouse process) and $G_d(t)$ describes the disentanglement process of the chains. For the Rouse process, the linear mixing rule⁴⁶ is adopted as,

$$G_R(t) = \sum_{i=A,B} \phi_i g_R^i(t) \quad (7)$$

The 'double reptation' rule offers much better agreement with experimental data than the 'linear mixing rule' for disentanglement process, hence a quadratic mixing rule is suggested in the form^{47,48} of

$$G_d(t) = \left(\sum_{i=A,B} \phi_i \sqrt{g_d^i(t)} \right)^2 \quad (8)$$

where $g_R^i(t)$ and $g_d^i(t)$ are the linear-viscoelastic relaxation moduli of different components, which may be expressed by the exponential functions of the elastic modulus (G_R^i, G_d^i) and the relaxation times (τ_R^i, τ_d^i)⁴⁸. After this treatment, the viscoelastic stress $\sigma_{\text{ve}}(\vec{r}, t)$ is calculated from the sum of three parts, the contribution of the component A and B, and a mixing term representing the interaction of both components:

$$\sigma_{\text{ve}} = \sum_{i=AA, BB, AB} G_i \mathbf{W}_i \quad (9)$$

In this representation the quantity \mathbf{W}_i is the viscoelastic strain and stress $G_i \mathbf{W}_i$ is parameterized by the elastic modulus G_i . According to the mixing rules, the elastic modulus can be expressed as $G_{AA} = \phi_A G_R^A + \phi_A^2 G_d^A$, $G_{BB} = \phi_B G_R^B + \phi_B^2 G_d^B$ and $G_{AB} = 2\phi_A \phi_B \sqrt{G_d^A G_d^B}$. Accordingly the relaxation times can be written as $\tau_d^{AA} = \tau_d^A$, $\tau_d^{BB} = \tau_d^B$ and $\tau_d^{AB} = 2\tau_d^A \tau_d^B / (\tau_d^A + \tau_d^B)$. For the Rouse time, there is no interactive part, so $\tau_R^{AA} = \tau_R^A$, $\tau_R^{BB} = \tau_R^B$ and $\tau_R^{AB} = 0$.

After applying the mixing rules to the Rolie-Poly constitutive model, the evolution equation of viscoelastic strain \mathbf{W}_i may be written as³³,

$$\begin{aligned} \frac{D\mathbf{W}_i}{Dt} = & 2D + (\nabla \vec{v}_T)^T \cdot \mathbf{W}_i + \mathbf{W}_i \cdot (\nabla \vec{v}_T) \\ & - \frac{1}{\tau_d^i} \mathbf{W}_i - f_1^i (I + \mathbf{W}_i + f_2^i \mathbf{W}_i) \end{aligned} \quad (10)$$

where $D = \frac{1}{2} (\nabla \vec{v}_T + (\nabla \vec{v}_T)^T)$ and the material derivative, $\frac{D\mathbf{W}_i}{Dt}$, is defined in terms of the tube velocity as $\frac{D\mathbf{W}_i}{Dt} = \frac{\partial \mathbf{W}_i}{\partial t} + \vec{v}_T \cdot$

$\nabla \mathbf{W}_i$; the coefficients involving the trace of the strain tensor are defined by

$$f_1^i = \frac{2}{\tau_R^i} \left(1 - \left(1 + \frac{\text{tr}(\mathbf{W}_i)}{3}\right)^{-\frac{1}{2}}\right) \quad \text{for } i = AA, BB \quad (11)$$

$$f_2^i = \beta \left(1 + \frac{\text{tr}(\mathbf{W}_i)}{3}\right)^\delta \quad \text{for } i = AA, BB \quad (12)$$

for \mathbf{W}_{AB} , as $\tau_R^{AB} \rightarrow 0$ leading to a non-stretching limit²⁸, the expressions are given by

$$f_1^{AB} = \frac{2}{3} [(\nabla \vec{v}_T) \cdot \text{tr}(\mathbf{W}_i + I)] \quad (13)$$

$$f_2^{AB} = \beta \quad (14)$$

We assume, for simplicity, that the components are of equal density, ρ . The motion of an incompressible, isothermal viscoelastic binary fluid is governed by the continuity equation

$$\vec{\nabla} \cdot \vec{v} = 0 \quad (15)$$

and the osmotic pressure and the viscoelastic stress are brought into the momentum balance equation,

$$\eta_0 \nabla^2 \vec{v} - \vec{\nabla} p - (\phi_A - \phi_B) \vec{\nabla} \mu + \vec{\nabla} \cdot \boldsymbol{\sigma}_{\text{ve}}(\vec{r}, t) = 0 \quad (16)$$

where p is the pressure field, and the Newtonian stress with viscosity η_0 can be a contribution from the solvent or from energy dissipation processes much faster than the slowest viscoelastic dynamics governed by the time-dependent viscoelastic stress tensor $\boldsymbol{\sigma}_{\text{ve}}(\vec{r}, t)$.

The equations above complete the Flory-Huggins-Rolie-Poly(FH-RP) fluid model in this study. The parameter β is the CCR magnitude coefficient and δ is an exponent to quantify the CCR. For simplicity, but without much loss of generality, the same value for β and δ for the three parts of $\boldsymbol{\sigma}_{\text{ve}}$ is assumed. By exploring the parameter space of the FH-RP model in terms of η_0 , τ_R^A , τ_d^A , τ_R^B , τ_d^B , G_R^A , G_d^A , G_R^B , G_d^B ($G_i = G_R^i + G_d^i$) and shear rate, the details of nonlinear dynamic behaviour in shear-induced phase transition of polymer mixtures could be systematically studied.

3 Numerical Methods

The governing equations of the FH-RP model are discretized through finite volume method (FVM) using an open source OpenFOAM CFD toolbox released by OpenCFD Ltd. The finite volume method ensures that the physical conservation laws are locally satisfied, through computing each term of the governing equations by volume integral over a control volume. For those terms involving divergence operators, volume integral can be converted to surface integral over the surfaces of

the control volume by applying the Gauss theorem. The resulting expressions are then discretised using appropriate differencing schemes. Gauss MINMOD and Gauss linear are applied in the discretisation scheme for the spatial discretization terms, and the temporal term is discretised using the simple Euler scheme. The above discretisation produces a system of linear equations to relate the cell face values of the unknown field variables at current time to their values at previous time and at the neighbouring cell centres. The system can be solved by one of the iterative matrix solvers, including the conjugate (PCG) and bi-conjugate gradient (PBICG) methods, available in the OpenFOAM toolbox. The details on how to use it can be found in the OpenFOAM manual⁴⁹.

The iterative solution algorithm used in this paper is a PISO-based algorithm, which have been well tested in a numerical study for the dynamics of polymer solutions in contraction flow⁵⁰. The numerical method involves a modification to the standard PISO algorithm by introducing polymer stress and the chemical potential unknowns into the momentum equation, as a part of the source term. In the absence flow, our simulation could reproduce the equilibrium phase behavior defined by the Flory-Huggins mixing free energy functional. Also the simulation results of homogeneous fluids under shear flow converge to the solution of the constitutive model with satisfactory accuracy. Moreover a similar OpenFOAM based viscoelastic flow solver has been critically validated under benchmark flow problems⁵⁰.

We summarised the key procedure of the iterative algorithm as follows:

- Step 1** Assuming $v^{n+1} = v^n$, integrate the constitutive equations implicitly to get the polymer viscoelastic stress components, $\boldsymbol{\sigma}_{\text{ve}}(\vec{r}, t)^{n+1}$.
- Step 2** Compute the force field $\vec{\nabla} \mu$ and $\vec{\nabla} \cdot \boldsymbol{\sigma}_{\text{ve}}$, then solve Eq. (1) to get ϕ_A^{n+1} .
- Step 3** Solve the momentum equation without the contribution of the pressure gradient term to obtain the estimated velocity components U^{n+1} .
- Step 4** Use the estimated velocity U^{n+1} to solve the pressure-correction equation of PISO algorithm, get the pressure field p^{n+1} .
- Step 5** Use the estimated pressure field p^{n+1} to calculate the corrected velocity field v^{n+1} .
- Step 6** Use the corrected velocity field v^{n+1} to solve the constitutive equation and the composition field evolving equation (Eq. (1)) again to get the corrected stress field and the corrected composition field.
- Step 7** Repeat the steps 3-6, using the corrected variable v^{n+1} , p^{n+1} , $\boldsymbol{\sigma}_{\text{ve}}(\vec{r}, t)^{n+1}$ and ϕ_A^{n+1} as improved estimates until

all corrections are negligibly small for the solutions at the present time.

Step 8 Repeat from the step 1 and advance to the next time step.

Here the superscript n and $n+1$ represent the past and the present times, respectively. The numerical scheme solves the non-linear governing equations in time and it is capable of modeling the unsteady flow.

4 Results and discussions

The maximum lattice size of two-dimensional simulation box in square shape is set to 256^2 . The top and bottom boundaries are physical walls and periodic boundary condition is applied to the other two sides of the box. Care has been taken in all simulations to ensure that there are sufficient lattice sites (seven at least) across the sharpest interfaces and also that the simulation results are independent of any further refinement of lattice density. Note also that these simulations cannot reproduce any physical structure with length scale larger than the simulation box.

For simplicity but without much loss of generality, the parameters are set as: $M_A = M_B = 1$, $k_B T = 1.3$, $\Gamma = 1$, $\zeta = 0.1$, $\eta_0 = 0.1$. Thus the equilibrium phase diagram is always symmetric with respect to $\phi_A = 0.5$. The critical point is at $\chi = 2$. Therefore, $\chi = 1.0$ for the FH-RP fluid means far away from the phase-coexistent region at equilibrium and the fluid is homogeneous for the entire composition range at this temperature.

A Gaussian random noise with an intensity of 10^{-3} was superimposed on a specified initial uniform composition field $\phi_A^0 = 0.5$ in all simulations reported here. Each component of the viscoelastic stress tensor σ_{ve} , including $\sigma_i, i = 1, 2, 3$, are initially set to zero. A wall velocity of $U_0 = \dot{\gamma}(L/2)$ is applied to the top and bottom walls in equal speed and opposite direction to achieve a required shear rate $\dot{\gamma}$, where L is characteristic length (distance between the walls).

By choosing appropriate values for the parameters β , δ , G_i , τ_d^i and τ_R^i , the FH-RP model exhibits different constitutive behaviour. Both of the monotonic and non-monotonic constitutive relationships will be analyzed in the following sections.

4.1 Interface instabilities with a monotonic constitutive equation

The CCR magnitude coefficient β is a control parameter on the monotonicity of the constitutive equation and can be fitted from experimental data. In comparison with the prediction of the full molecular theory for polymer melts, Likhtman and Graham²⁸ used $\beta = 0.5$ for the transient data and $\beta = 1$ for the steady state data. However in order to obtain a good fit of the

experimental data, they suggest that a small value for the CCR parameter β should be used. Adams and Olmsted tune the parameter between 0.5 and 1 to generate either non-monotonic or monotonic constitutive behaviour^{30,33}. They usually set $Z = \frac{\tau_d}{3\tau_R} > 260$, which is much higher than the values needed to observe phase separation experimentally, and $\beta > 0.5$ to obtain constitutive curve with a broad plateau.

Kabanemi and Chung^{31,32} set a much lower value of β , and in some cases $\beta = 0$ to produce non-monotonic constitutive curve. In general, the value of β should be determined from experimental data, hence allow the FH-RP model to capture various physical features of complex fluids.

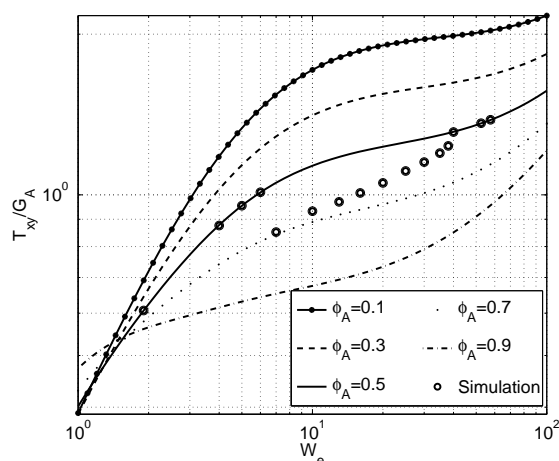


Fig. 1 The scaled steady-state shear stress T_{xy} versus $We = \dot{\gamma}\tau_d^A$ calculated by the homogeneous FH-RP model of various ϕ_A , as indicated, with parameters $\beta = 0.2$, $G_A = 1.0$, $G_B = 4.0$, $\frac{\tau_d^A}{\tau_R^A} = 20$ and $\frac{\tau_d^B}{\tau_R^B} = 200$.

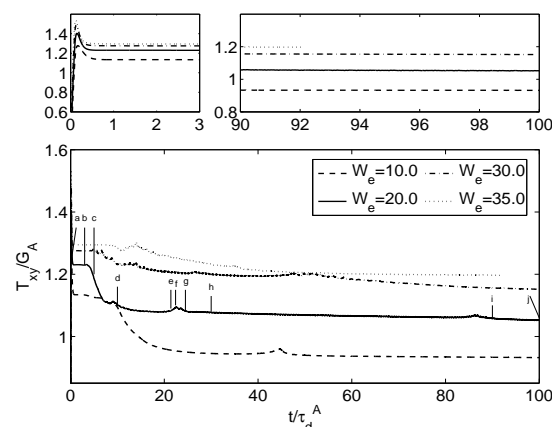
The simulation results presented in this section are obtained by setting the model parameters $\beta = 0.2$ and $\delta = -0.5$, $G_A = 1.0$ ($G_R^A = 0.1, G_d^A = 0.9$), $G_B = 4.0$ ($G_R^B = 0.2, G_d^B = 3.8$), $\tau_R^A = 1.0$, $\tau_R^B = 0.01$, $\frac{\tau_d^A}{\tau_R^A} = 20$, and $\frac{\tau_d^B}{\tau_R^B} = 200$ (i.e., $Z_A = 6.67$, $Z_B = 66.67$). Those parameters give a strictly monotonic constitutive equation for all values of ϕ_A , and define a binary polymeric system which is miscible under equilibrium condition and shows shear-induced phase separation in a range of shear rates. The steady state solutions of the model are calculated by solving Eq.(9) to Eq.(14) under a fixed composition field ϕ_A using the pre-defined ODE solvers available in MATLAB and are shown in Fig. 1. The absolute differences between the numerical results obtained from the OpenFOAM solver and the MATLAB calculation for a homogenous Rolie-Poly fluid are less than 0.003.

With this set of the parameters, all the constitutive curves of homogenous fluid under various ϕ_A are monotonic as in-

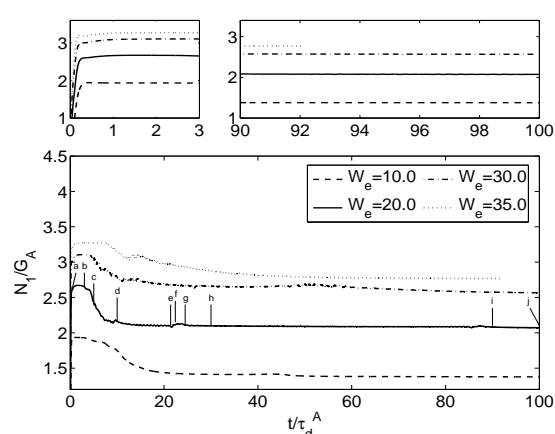
indicated in Fig. 1. There is no intrinsic constitutive instability. Under low shear rate ($W_e \lesssim 6.0$), the calculated shear stress and first normal stress difference exactly match the corresponding analytical results of homogeneous fluid ($\phi_A = 0.5$). The phase separation only occurs in a range of shear rates: $7.0 \lesssim W_e \lesssim 38.0$, in which the homogeneous phase with initial small composition fluctuation separates into A-component-rich and B-component-rich phases in a form of shear bands. In the higher shear rate region of $W_e \gtrsim 40.0$, the simulation results again coincide with the analytical calculations for a homogeneous fluid and no phase separation is observed over the duration of our simulations. Fig. 1 shows that no stress plateau exists. It was also reported in the previous study of the FH-JS model^{24,25} and a liquid crystalline model⁵¹.

The transient behaviour corresponding to several points in Fig. 1 are presented in Fig. 2(a) for shear stress and Fig. 2(b) for first normal stress difference. Within the phase separation region, the numerical results of the shear stress and the first normal difference coincide with the theoretical solution of a homogeneous FH-RP fluid but then turn into a two-phase solution as a significant drop (the second drop in shear stress) of T_{xy} and N_1 appears. It takes as long as $70\tau_A$ to reach a steady state.

Snapshots of the composition field at several instant during phase separation for the case of $W_e = 20.0$ have been shown in Fig. 4. The evolution of the shear rate field and the stress field follow the same pattern as that of the composition field shown in the figure. The letters *a* to *j* mark the points along the transient stress curves in Fig. 2 which refer to the individual images in Fig. 4, respectively. From the evolution of composition field, there are two dynamical mechanisms by which the shear bands reach to a steady state: diffusive mechanism and convective through wave instability. They have also been observed in a 30/70 polymer mixture²⁴, but only a purely diffusive mechanism was seen in 50/50 polymer mixtures²⁵. At $t = 0$, the composition is homogeneous. The significantly stress dropping between points *b* and *d* in Fig. 2, corresponding to Fig. 4(b)-4(d), shows the direct formation of fine composition bands by nucleation and unstable wave structure interacting with each other. At point *d*, the stress has reached a low plateau but the composition field is still unstable. As approaching to the steady state, there is an interesting dynamical process observed between point *e* and *g* referring to the snapshots shown in Fig. 4(e)-4(g): a wave structure breaks up forming droplet, then the droplet interacts with the remaining bands and subsequently forms into a coarser band. This phenomenon explains the stress fluctuations in Fig. 2; It is not only seen in this specific case for $W_e = 20.0$, but also for all the cases shown in Fig. 2, fluctuations always appear along with a process breaking wave into droplet then to much coarser band. From $t = 30\tau_A$, the band structures gradually grow via diffusive mechanism, and shortly after the small oscillation



(a) Transient shear stress



(b) Transient first normal stress difference

Fig. 2 Transient shear stress and first normal stress difference for various values of the Weissenberg number W_e with parameters: $\beta = 0.2$, $G_A = 1.0$, $G_B = 4.0$, $\frac{\tau_d^A}{\tau_R^A} = 20$ and $\frac{\tau_d^B}{\tau_R^B} = 200$

around $t = 85\tau_A$ corresponding to another wave to droplet process, the shear bands get much coarser and far away from each other. From $t = 100\tau_A$, the remaining bands change very little and reach the steady state.

It is worth to note that our numerical results show a dynamic steady state, unlike the previous studies presenting a strictly smooth shear bands with J-S model^{24,25}, there are wavy band structures moving with the flow without further coarsening. Fig. 3 shows the composition profiles across the simulation box. As seen in the top figure, the fluid formed into band structures and the maximum value of ϕ_A is less than 0.8 in steady state. In order to reveal structural evolution of the unstable interfaces, we plot the composition profile along the flow di-

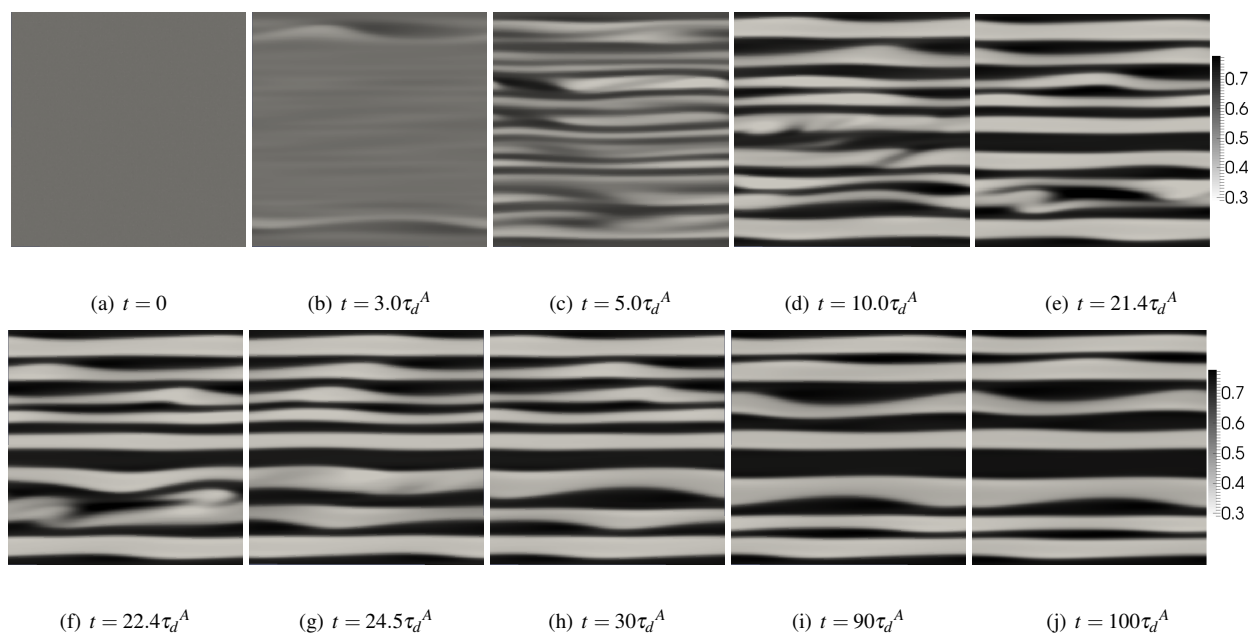


Fig. 4 Snapshots of the composition field ϕ_A at various instant t for an initially homogeneous viscoelastic binary fluid of $\mathcal{W}_e = 20.0$, $\beta = 0.2$, $G_A = 1.0$, $G_B = 4.0$, $\frac{\tau_d^A}{\tau_R^A} = 20$ and $\frac{\tau_d^B}{\tau_R^B} = 200$

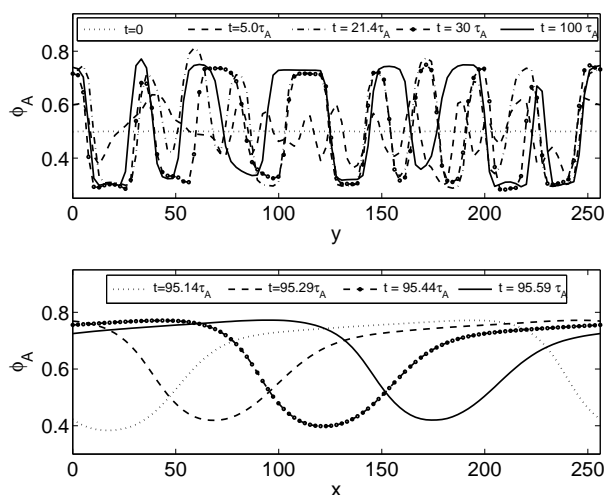


Fig. 3 The composition profiles across the simulation box for a binary fluid of $\mathcal{W}_e = 20.0$ with $\beta = 0.2$, $G_A = 1.0$, $G_B = 4.0$, $\frac{\tau_d^A}{\tau_R^A} = 20$ and $\frac{\tau_d^B}{\tau_R^B} = 200$. (Top) Snapshots of composition along the shear gradient (y) direction; (Bottom) Snapshots of composition along the flow direction (x) near the band interface ($y = 64$) in the steady state

rection near the band interfaces, as shown in the bottom figure of Fig. 3, which presents a typical moving pattern: a wavy structure moves along the flow direction.

Recently, a growing body of data reveals that the shear bands can fluctuate. Most of the observations suggest a wavy structure oscillating between two bands. Many experimental results identify such fluctuations in complex fluids^{9,52–57} and the interface instabilities have also been observed in numerical studies with a diffusive J-S model^{27,55,58} and a two-species model⁵⁹. The simulation results demonstrate that the proposed FH-RP model can capture the essential instabilities in complex fluids through a thermodynamically consistent way.

4.2 Chaotic rheological responses with a non-monotonic constitutive equation

In this section, we numerically study the dynamic phase separations in polymer mixtures with a typical non-monotonic constitutive equation. To generate a non-monotonic constitutive curve with a wide range of ϕ_A , the model parameters are set as: $\beta = 0$ and $\delta = -0.5$, $G_A = G_B = 2.5$, $\tau_R^A = 0.2$, $\tau_R^B = 0.01$, $\frac{\tau_d^A}{\tau_R^A} = 100$ and $\frac{\tau_d^B}{\tau_R^B} = 250$. This defines a binary polymeric system with a non-monotonic constitutive behaviour. It is miscible under equilibrium condition.

The intrinsic constitutive curves of various values of ϕ_A have been presented in Fig. 5, all of which are non-monotonic. The numerical simulation results of the shear stress have also

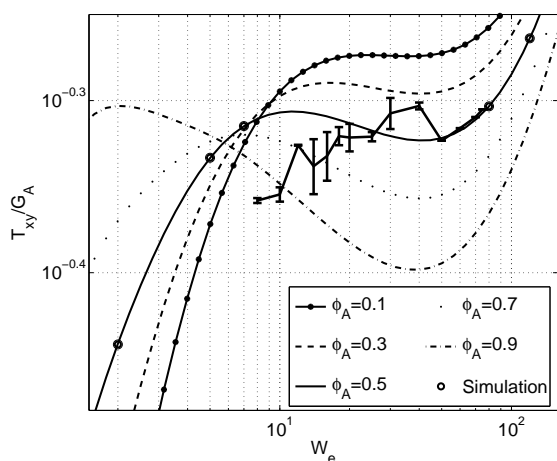
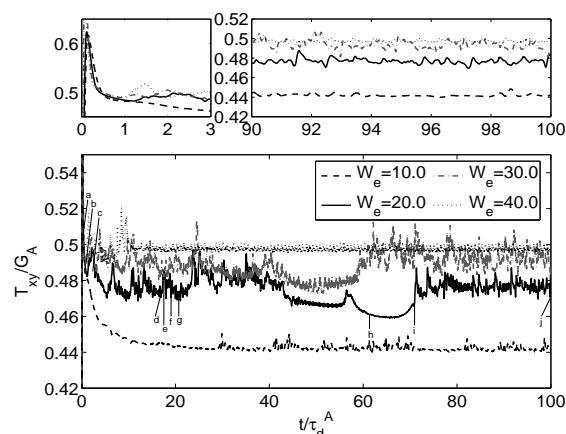


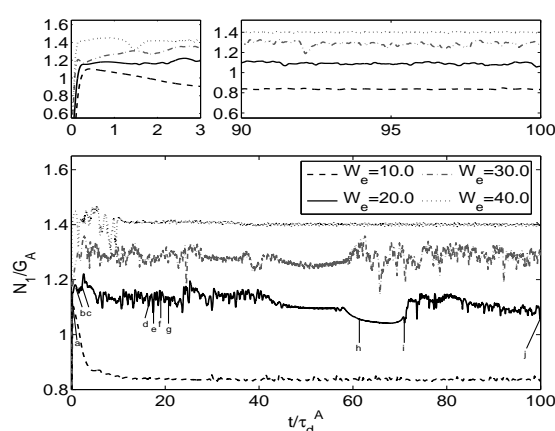
Fig. 5 (Vertical bars) Fluctuation range of T_{xy} versus scaled shear rate $\mathcal{W}_e = \dot{\gamma}\tau_d^A$ for shear-induced phase separation with parameters $\beta = 0$, $G_A = G_B = 2.5$, $\frac{\tau_d^A}{\tau_R} = 100$ and $\frac{\tau_d^B}{\tau_R} = 250$, along with the corresponding constitutive curves for homogeneous FH-RP fluids of various values of ϕ_A , as indicated.

been plotted in this figure. In the homogeneous range for low shear rate ($\mathcal{W}_e \lesssim 7.0$) and high shear rate ($\mathcal{W}_e \gtrsim 80$), the simulation results exactly coincide with the FH-RP constitutive curve in a homogeneous state, which are indicated by the circles in Fig. 5. Similar to the monotonic case, in the region of $8 \lesssim \mathcal{W}_e \lesssim 77$, flow-induced phase separation takes place and the stress deviation is observed. Different from previous cases in which the shear stress always can reach a steady state, in this system the stress does not reach a steady value, but continuously fluctuates. The fluctuation range of the shear stress is indicated with the vertical error bars in Fig. 5. Another significant difference is that the flow curve of shear stress versus shear rate is not linear as the monotonic case, but exhibits some wavy structure within the phase separation region. This may attribute to the large fluctuations in the simulations. In order to check whether or not the final state achieved here, it is necessary to use a much larger simulation box and this will form part of our future research. However, in an experimental study of associative polymer networks, Sprakel¹¹ presented similar fluctuations of the flow curves and their work revealed rheochaos of the transient stress response, which is similar to our simulation results.

The transient behaviour of the stress components at various shear rates corresponding to several points in Fig. 5 are shown in Fig. 6(a) for shear stress T_{xy} and Fig. 6(b) for first normal stress difference N_1 . Under low shear rate ($\mathcal{W}_e = 10$), the magnitude of the fluctuation is small. In the middle of the phase separation region, such as $\mathcal{W}_e = 20$ and $\mathcal{W}_e = 30$, the fluctuations become much larger. In even higher shear rate region, the



(a) Transient shear stress



(b) Transient first normal stress difference

Fig. 6 Transient shear stress and first normal stress difference revealing rheochaos for various values of the Weissenberg number \mathcal{W}_e with parameters: $\beta = 0$, $G_A = G_B = 2.5$, $\frac{\tau_d^A}{\tau_R} = 100$ and $\frac{\tau_d^B}{\tau_R} = 250$

stress oscillation reduces as shown in the case of $\mathcal{W}_e = 40$. If looking into the detailed evolutions of the transient behaviour of the stresses, it reveals some special patterns. For $\mathcal{W}_e = 40$, the stress continuously oscillates with the same amplitude and periodically repeats similar patterns. Surprisingly, the case of $\mathcal{W}_e = 20$ shows a quite difference behaviour. Except for the larger fluctuations, there is a quiet region in which the stress oscillation vanishes.

Snapshots of the composition field during phase separation for the case of $\mathcal{W}_e = 20$ with a non-monotonic constitutive curve are shown in Fig. 7. The letters $a - j$ marked in Fig. 6 refer to the individual images in Fig. 7 and indicate the points along the transient stress curves corresponding to each image.

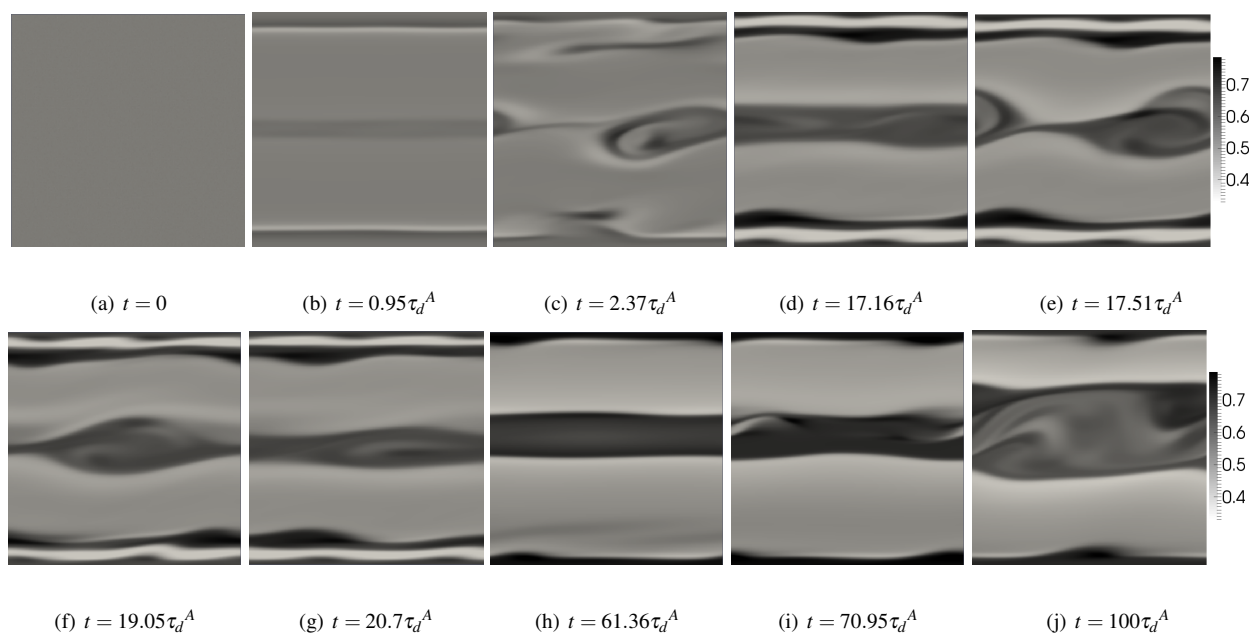


Fig. 7 Snapshots of the composition field ϕ_A at various times t for an initially homogeneous viscoelastic binary fluid of $\mathcal{W}_e = 20.0$, with parameters: $\beta = 0$, $G_A = G_B = 2.5$, $\frac{\tau_d^A}{\tau_R^A} = 100$ and $\frac{\tau_d^B}{\tau_R^B} = 250$

At $t = 0$, the composition is homogeneous with a small random noise. After the initial stress overshoot, at $t = 0.95\tau_d^A$, the composition field forms smooth band structures. Shortly it is found that the flat bands have been broken as shown in Fig. 7(c). From here, the chaotic stress response emerges, and typical phase transitions corresponding to the rheochaos can be seen in Fig. 7(d) to 7(g). At the beginning, the bands stay with unstable interfaces, then a vortex structure emerges within the central band, and this turbulence gradually subsides at $t = 20.7\tau_d^A$. We plot the snapshots of streamlines in Fig. 8 between $t = 17.16\tau_d^A$ and $t = 20.7\tau_d^A$, from which we can find a symmetric vortex clearly appearing within the central band. This process repeats for a long period and leads to large fluctuations in stress curves. Although the results in an experimental study of telechelic polymers¹¹ suggest that the fluctuating stress is caused by interface instabilities, our simulations reveal another possible cause: the vortex instability inside the band structure. We hope more visualization experiments could be conducted to confirm our observations in the future.

At $t = 61.36\tau_d^A$, corresponding to a smooth region of the stress curves showed in Fig. 6, the band structures also form a more stable state in Fig. 7(h): the central band becomes uniform with a smooth interface, and the fine bands near the wall combine into darker ones after interacting with each other. This smooth region terminates at around $t = 70.95\tau_d^A$, thus the stress curves come back to the fluctuations. The composition field has been shown in Fig. 7(i) and 7(j). It is seen

that instabilities emerge within the central band, and it is still unstable by $t = 100\tau_d^A$. This particular intermittent rheochaos has not been observed in the numerical studies with a FH-JS model.

The visual impression of this vortex structure shown in Fig. 7 and Fig. 8, are observed in all of the cases with large rheological fluctuations. A more careful analysis is presented in Fig. 9. It shows the average Fourier spectra of the intensity reflected by composition field along the velocity direction in the central of the simulation box, which exhibits power law decay over one decade of frequency. Similar to the case of elastic turbulence^{60,61}, the power spectrum in wave vector seems to approximately follow a power law up to $k_d \sim 33(\Delta x)^{-1}$, where $\Delta x = \frac{L}{256}$ is the lattice size in this study. The case of $\mathcal{W}_e = 10$ shows significant difference from other cases in Fig. 9, as indicated in the figure, the critical value $k_d' < k_d$. Compared to other cases, with $\mathcal{W}_e = 10$, we find that the stress fluctuation is relatively small and the shear bands are more stable, and this also leads to a much smaller vortex structure in the streamline plot. Since k_d^{-1} is related to the stress correlation length, we may conclude that larger vortex and rheological fluctuations are relevant to a smaller stress correlation length.

5 Conclusions

The two fluid model directly couples the viscoelastic stress and the diffusive fluid composition, thus there is no need to

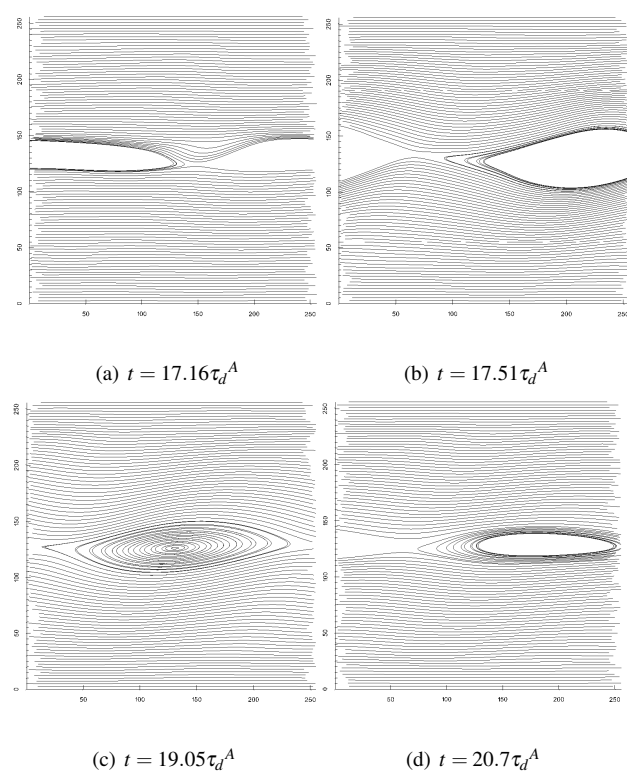


Fig. 8 Snapshots of streamlines corresponding to typical rheochaos, which clearly show a vortex structure emerges for an initially homogeneous viscoelastic binary fluid of $W_e = 20.0$

introduce any diffusive stress term into the constitutive equations. In this study, we extend the FH-JS model by integrating with Rolie-Poly constitutive model. Two-dimensional simulations have been carried out and the numerical results for a typical monotonic and non-monotonic constitutive equation are analyzed respectively, which show that our model can capture the essential features of the shear-induced phase transitions in binary polymer mixtures.

The simulations reproduce many dynamic phenomena reported in literature, including the steady-state shear-banding, the interface instabilities between the bands, and the dynamic mechanisms to reach stable band structures. With a non-monotonic constitutive equation, we have also observed that the band structures are strongly unstable both in time and in space. The stress continuously fluctuates in a chaotic manner. The correlations between microstructure evolution and chaotic rheological responses have been identified. Other than the interface instability, our results reveal another possible cause of the rheochaos: a vortex structure emerges within the central band.

Coupled with a realistic constitutive model, the computational model presented here could provide valuable guidance

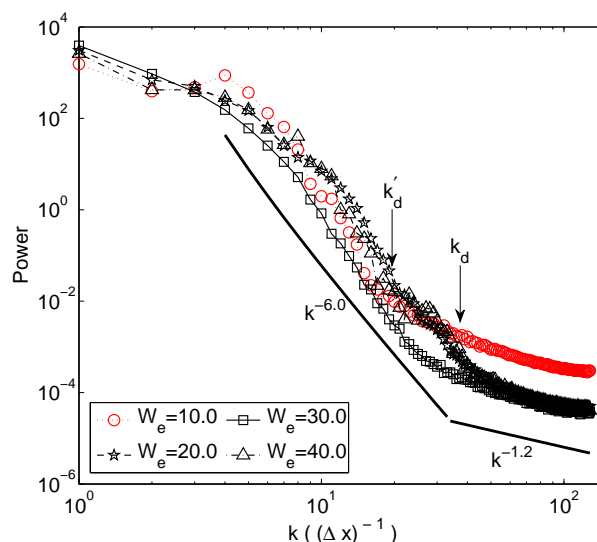


Fig. 9 Average Fourier spectra for various W_e obtained on the wave vector domain by computing Fourier transforms of the intensity reflected by the composition field along the velocity direction at the middle point, and then by averaging for different times. The two solid lines are $k^{-6.0}$ and $k^{-1.2}$ fit respectively.

to new experimental work and could also be used to quantitatively study some outstanding problems by appropriately selecting the parameters to mimic the real physical systems. Motivated by many experimental observations, we hope to address an in-depth quantitative study of the rheochaos in complex fluids in future simulations, including large-scale three-dimensional simulations.

Acknowledgments

This work is partially supported by BBSRC grant (B-B/K011146/1) in UK, the National Natural Science Foundation of China (Grant No.61221491, No.61303071 and No. 61120106005), and Open fund from State Key Laboratory of High Performance Computing (No. 201303-01).

References

- 1 A. Silberberg and W. Kuhn, *Nature*, 1952, **170**, 450–451.
- 2 D. Jou, J. Casasvazquez and M. Criadosancho, *Physical Properties of Polymers*, 1995, **120**, 207–266.
- 3 A. Onuki, *Journal of Physics: Condensed Matter*, 1997, **9**, 6119.
- 4 M. Laurati, G. Petekidis, N. Koumakis, F. Cardinaux, A. B. Schofield, J. M. Brader, M. Fuchs and S. U. Egelhaaf, *Journal of Chemical Physics*, 2009, **130**, 134907.
- 5 S. Lerouge and J. F. Berret, *Polymer Characterization: Rheology, Laser Interferometry, Electrooptics*, 2010, **230**, 1–71.
- 6 B. Lonetti, M. Camargo, J. Stellbrink, C. N. Likos, E. Zaccarelli, L. Will-

- ner, P. Lindner and D. Richter, *Physical Review Letters*, 2011, **106**, 228301.
- 7 S. Ravindranath, S. Q. Wang, M. Olechnowicz, V. S. Chavan and R. P. Quirk, *Rheologica Acta*, 2011, **50**, 97–105.
- 8 J. Y. Lee, G. G. Fuller, N. E. Hudson and X.-F. Yuan, *Journal of Rheology (1978-present)*, 2005, **49**, 537–550.
- 9 R. Angelico, C. O. Rossi, L. Ambrosone, G. Palazzo, K. Mortensen and U. Olsson, *Physical Chemistry Chemical Physics*, 2010, **12**, 8856–8862.
- 10 S. Manneville, A. Colin, G. Waton and F. Schosseler, *Physical Review E*, 2007, **75**, 061502.
- 11 J. Sprakel, E. Spruijt, M. A. C. Stuart, N. A. M. Besseling, M. P. Lettinga and J. van der Gucht, *Soft Matter*, 2008, **4**, 1696–1705.
- 12 T. Divoux, D. Tamarit, C. Barentin and S. Manneville, *Physical Review Letters*, 2010, **104**, 208301.
- 13 P. E. Boukany and S. Q. Wang, *Journal of Rheology*, 2009, **53**, 73–83.
- 14 P. E. Boukany, Y. T. Hu and S. Q. Wang, *Macromolecules*, 2008, **41**, 2644–2650.
- 15 P. E. Boukany and S. Q. Wang, *Macromolecules*, 2010, **43**, 6950–6952.
- 16 C. Domb, *Phase transitions and critical phenomena*, Access Online via Elsevier, 2000, vol. 19.
- 17 H. Ji and E. Helfand, *Macromolecules*, 1995, **28**, 3869–3880.
- 18 N. Clarke and T. C. B. McLeish, *Physical Review E*, 1998, **57**, R3731–R3734.
- 19 S. T. Milner, *Physical Review E*, 1993, **48**, 3674–3691.
- 20 P. Stansell, K. Stratford, J. C. Desplat, R. Adhikari and M. E. Cates, *Physical Review Letters*, 2006, **96**, 085701.
- 21 K. Stratford, J.-C. Desplat, P. Stansell and M. Cates, *Physical Review E*, 2007, **76**, 030501.
- 22 S. M. Fielding, *Physical Review E*, 2008, **77**, 021504.
- 23 X. F. Yuan and L. Jupp, *Europhysics Letters*, 2002, **60**, 691–697.
- 24 L. Jupp and X. F. Yuan, *Journal of Non-Newtonian Fluid Mechanics*, 2004, **124**, 93–101.
- 25 L. Jupp, T. Kawakatsu and X. F. Yuan, *Journal of Chemical Physics*, 2003, **119**, 6361–6372.
- 26 S. M. Fielding and P. D. Olmsted, *Physical Review Letters*, 2003, **90**, 224501.
- 27 S. M. Fielding and P. D. Olmsted, *Physical Review Letters*, 2006, **96**, 104502.
- 28 A. E. Likhtman and R. S. Graham, *Journal of Non-Newtonian Fluid Mechanics*, 2003, **114**, 1–12.
- 29 R. S. Graham, A. E. Likhtman and T. C. B. McLeish, *Journal of Rheology*, 2003, **47**, 1171–1200.
- 30 J. M. Adams and P. D. Olmsted, *Physical Review Letters*, 2009, **102**, 067801.
- 31 K. K. Kabanemi and J. F. Hetu, *Rheologica Acta*, 2009, **48**, 801–813.
- 32 C. Chung, T. Uneyama, Y. Masubuchi and H. Watanabe, *Rheologica Acta*, 2011, **50**, 753–766.
- 33 J. M. Adams, S. M. Fielding and P. D. Olmsted, *Journal of Rheology*, 2011, **55**, 1007–1032.
- 34 M. Cromer, M. C. Villet, G. H. Fredrickson and L. G. Leal, *Physics of Fluids*, 2013, **25**, 051703.
- 35 R. Bandyopadhyay, G. Basappa and A. K. Sood, *Physical Review Letters*, 2000, **84**, 2022–2025.
- 36 L. Becu, S. Manneville and A. Colin, *Physical Review Letters*, 2004, **93**, 018301.
- 37 R. Ganapathy and A. K. Sood, *Physical Review Letters*, 2006, **96**, 108301.
- 38 S. Manneville, J. B. Salmon and A. Colin, *European Physical Journal E*, 2004, **13**, 197–212.
- 39 L. Gentile, B. F. B. Silva, S. Lages, K. Mortensen, J. Kohlbrecher and U. Olsson, *Soft Matter*, 2013, **9**, 1133–1140.
- 40 B. Chakrabarti, M. Das, C. Dasgupta, S. Ramaswamy and A. K. Sood, *Physical Review Letters*, 2004, **92**, 055501.
- 41 S. M. Fielding and P. D. Olmsted, *Physical Review Letters*, 2004, **92**, 084502.
- 42 M. Doi and A. Onuki, *Journal De Physique II*, 1992, **2**, 1631–1656.
- 43 H. Ji and E. Helfand, *Macromolecules*, 1995, **28**, 3869–3880.
- 44 H. Tanaka, *Physical Review Letters*, 1993, **71**, 3158–3161.
- 45 B. M. Forrest and R. Toral, *Journal of Statistical Physics*, 1994, **77**, 473–489.
- 46 E. van Ruymbeke, J. Nielsen and O. Hassager, *Journal of Rheology*, 2010, **54**, 1155–1172.
- 47 J. Descloizeaux, *Europhysics Letters*, 1988, **5**, 437–442.
- 48 E. van Ruymbeke, C.-Y. Liu and C. Bailly, *Rheology Reviews*, 2007, 53–134.
- 49 *OpenFOAM programmer's guide*, 2013.
- 50 S. C. Omowunmi and X. F. Yuan, *Rheologica Acta*, 2013, **52**, 337–354.
- 51 P. D. Olmsted and C. Y. D. Lu, *Faraday Discussions*, 1999, **112**, 183–194.
- 52 M. R. Lopez-Gonzalez, W. M. Holmes, P. T. Callaghan and P. J. Photinos, *Physical Review Letters*, 2004, **93**, 268302.
- 53 S. Lerouge, M. Argentina and J. P. Decruppe, *Physical Review Letters*, 2006, **96**, 088301.
- 54 J. P. Decruppe, L. Becu, O. Greffier and N. Fazel, *Physical Review Letters*, 2010, **105**, 258301.
- 55 P. Nghe, S. M. Fielding, P. Tabeling and A. Ajdari, *Physical Review Letters*, 2010, **104**, 248303.
- 56 M. A. Fardin and S. Lerouge, *European Physical Journal E*, 2012, **35**, 178303.
- 57 M. A. Fardin, T. J. Ober, V. Grenard, T. Divoux, S. Manneville, G. H. McKinley and S. Lerouge, *Soft Matter*, 2012, **8**, 10072–10089.
- 58 S. M. Fielding and H. J. Wilson, *Journal of Non-Newtonian Fluid Mechanics*, 2010, **165**, 196–202.
- 59 M. Cromer, L. P. Cook and G. H. McKinley, *Journal of Non-Newtonian Fluid Mechanics*, 2011, **166**, 566–577.
- 60 A. Groisman and V. Steinberg, *Nature*, 2000, **405**, 53–55.
- 61 M. A. Fardin, D. Lopez, J. Croso, G. Gregoire, O. Cardoso, G. H. McKinley and S. Lerouge, *Physical Review Letters*, 2010, **104**, 178303.

The numerical results of RP-FH model reveal another possible cause of the rheochaos: a vortex structure emerges within the central band.

